16th World Congress in Computational Mechanics (WCCM)
21-26 July 2024, Vancouver, Canada
A. Korobenko, M. Laforest, S. Prudhomme, R. Vaziri (Eds)

STABILIZATION OF MIXED DISPLACEMENT-PRESSURE FINITE ELEMENTS AT FINITE STRAINS USING POLYHEDRAL FORMULATIONS AND VORONOI MESHING

B. SAUREN[1], E. OHEIM[1] AND S. KLINKEL[1*]

[1] Chair of Structural Analysis and Dynamics, RWTH Aachen University, Aachen, Germany

Key words: polyhedral finite elements, nonlinear analysis, inf-sup, spurious modes, Voronoi.

Abstract. The hexahedral mixed displacement-pressure finite element of the lowest order (H1/P0) has shown to be simple and effective during both linear and nonlinear analysis of incompressible solids. While the discrete displacement field is generally considered to be sufficiently accurate, the discrete pressure field can sometimes be heavily polluted by spurious pressure modes. This results from the fact that the element does not fulfill the inf-sup condition. While postprocessing techniques, such as pressure filtering or smoothing, exist to remove the spurious pressure modes from the solution, this contribution aims on the exclusion of spurious pressure modes from the solution *a priori* due to the element geometry. By employing polyhedral finite element formulations on Voronoi tessellations in three dimensions, we show that the discrete kernel of the linearized mixed bilinear form only consists of the hydrostatic pressure mode. A spurious pressure mode is automatically suppressed due to the vertex-to-volume ratio in the finite element mesh. These considerations hold for any arbitrary physically admissible displacement state that can occur within a Newton-Raphson framework. A nonlinear numerical example shows that spurious pressure modes are indeed suppressed if the type of tessellation is changed from hexahedral to Voronoi.

1 INTRODUCTION

The mechanical behavior of nearly-incompressible materials, such as polymers or biological tissue, can be described by their governing partial differential equations. Unfortunately, numerical problems arise if the equations are approximated in a finite-dimensional subspace using the irreducible form of the finite element method. As a result, the solution is severely underestimated, commonly referred to as volumetric locking. Several improvement methods have been developed to overcome these issues, see [1, 2, 3]. Here, we focus on the imposition of the volume constraint using a Lagrange multiplier [3] and aim to approximate the resulting displacement and pressure fields by their lowest-order approximation, i.e. using linear displacements and constant pressures. On most standard finite element meshes, the displacement solution generally turns out to be volumetric locking-free. The pressure field is, however, prone to display spurious pressure oscillations, rendering the pressure field as physically meaningless. In theory,

these problems occur because the Ladyzhenskaya-Babuška-Brezzi (LBB), or inf-sup condition, is not fulfilled [4, 5, 6].

In this contribution, we show that it is possible to fulfill the inf-sup condition using polyhedral finite element formulations combined with Voronoi meshing strategies. In fact, we use the exact same variational framework as the standard hexahedral H1/P0 element, but impose interpolation functions based on the scaled boundary parameterization [7, 8] to discretize the polyhedral element. Utilizing the properties of a three-dimensional Voronoi mesh, we can show that spurious pressure modes are suppressed and further stabilization of the element is not required. We herewith extend the theory presented in [9] to three-dimensional problems. A nonlinear numerical example is presented to show that the use of Voronoi meshes suppresses spurious pressure oscillations and can reproduce smoother pressure fields compared to classical mixed hexahedral finite elements.

2 LINEARIZED WEAK TWO-FIELD VARIATIONAL FORMULATION

A continuum domain $\Omega = \Omega_0 \subset \mathbb{R}^3$ is considered in the initial configuration at $t = 0$. Its boundary $\partial\Omega = \partial\Omega_D \cup \partial\Omega_N$ is partitioned into a Dirichlet boundary $\partial\Omega_D \subset \mathbb{R}^2$ and a Neumann boundary $\partial\Omega_N \subset \mathbb{R}^2$. Only hyperelastic and isotropic materials are considered throughout this work. To derive the mixed potential, the strain energy density function is split into a deviatoric and a volumetric part according to:

$$\begin{aligned} W(\mathbf{C}, J) &= W_{\text{dev}}(\mathbf{C}) + W_{\text{vol}}(J) \\ &= W_{\text{dev}}(\mathbf{C}) + \frac{\kappa}{2}\left[\hat{U}(J)\right]^2. \end{aligned} \tag{1}$$

As soon as a material becomes nearly-incompressible, $W_{\text{vol}}(J) \approx 0$. Consequently, the chosen penalty function $\hat{U}(J) = J - 1$ tends towards zero. The volume constraint is then incorporated into the problem using a perturbed Lagrangian formulation [3]. The total energy potential is extended as

$$\tilde{\Pi}(\mathbf{u}) = \Pi_{\text{int}} - \Pi_{\text{ext}} + \int_\Omega \left(p\,\hat{U}(J) - \frac{1}{2\kappa} p^2 \right) \mathrm{d}V, \tag{2}$$

where p is the hydrostatic pressure and acts as a Lagrange multiplier. Minimization of the potential corresponds to solving the weak formulation of the two-field saddle-point problem:

$$\underbrace{\int_\Omega \delta\mathbf{E} : \frac{\partial W_{\text{dev}}}{\partial \mathbf{E}}\,\mathrm{d}V + \int_\Omega \delta\mathbf{E} : \frac{\partial \hat{U}}{\partial \mathbf{E}}\,p\,\mathrm{d}V}_{G_u} = \underbrace{\int_\Omega \delta\mathbf{u}^{\mathsf{T}}\,\mathbf{f}\,\mathrm{d}V + \int_{\partial\Omega_N} \delta\mathbf{u}^{\mathsf{T}}\,\bar{\mathbf{t}}_0\,\mathrm{d}A}_{\delta\Pi_{\text{ext}}} \tag{3a}$$

$$\underbrace{\int_\Omega \delta p\,\hat{U}(J) \; - \int_\Omega \delta p\,\frac{1}{\kappa}\,p\,\mathrm{d}V}_{G_p} = 0. \tag{3b}$$

Here, $\mathbf{C}$ denotes the right Cauchy-Green deformation tensor, $\mathbf{f}$ the body force and $\bar{\mathbf{t}}_0$ the initial boundary traction vector. The term that includes κ in Eq. (3b) disappears in case of total incompressibility.

Since the variational formulation includes geometrical and material nonlinearities, a Newton-Raphson scheme is used to linearize the nonlinear problem. The linearized weak form of Eqs. (3) in the direction of the increments $\Delta\mathbf{u}$ and Δp reads:

$$\mathcal{D}_u G_u \cdot \Delta\mathbf{u} + \mathcal{D}_p G_u \cdot \Delta p = -G_u + \delta\Pi_{\text{ext}} \tag{4a}$$
$$\mathcal{D}_u G_p \cdot \Delta\mathbf{u} - \mathcal{D}_p G_p \cdot \Delta p = -G_p, \tag{4b}$$

with the directional derivatives

$$\mathcal{D}_u G_u \cdot \Delta\mathbf{u} = \int_\Omega \delta\mathbf{E} : \left(\frac{\partial^2 W_{\text{dev}}}{\partial\mathbf{E}\partial\mathbf{E}} + p\frac{\partial^2 \hat{U}}{\partial\mathbf{E}\partial\mathbf{E}} \right) : \Delta\mathbf{E}\,\mathrm{d}V + \int_\Omega \left(\frac{\partial W_{\text{dev}}}{\partial\mathbf{E}} + p\frac{\partial \hat{U}}{\partial\mathbf{E}} \right) : \Delta\delta\mathbf{E}\,\mathrm{d}V, \tag{5a}$$

$$\mathcal{D}_p G_u \cdot \Delta p = \int_\Omega \delta\mathbf{E} : \frac{\partial \hat{U}}{\partial\mathbf{E}}\,\Delta p\,\mathrm{d}V, \tag{5b}$$

$$\mathcal{D}_u G_p \cdot \Delta\mathbf{u} = \int_\Omega \delta p\,\frac{\partial \hat{U}}{\partial\mathbf{E}} : \Delta\mathbf{E}\,\mathrm{d}V, \tag{5c}$$

$$\mathcal{D}_p G_p \cdot \Delta p = \int_\Omega \delta p\,\frac{1}{\kappa}\,\Delta p\,\mathrm{d}V. \tag{5d}$$

3 DISCRETIZATION USING THE SCALED BOUNDARY PARAMETERIZATION

The domain Ω_h in the reference configuration is approximated using an arbitrary tessellation into n_E elements E which implies

$$\Omega \approx \Omega_h = \bigcup_{E=1}^{n_E} \mathcal{E}_E, \tag{6}$$

with element domain $\mathcal{E}_E \subset \Omega_h \subset \mathbb{R}^3$. Likewise, the approximated boundary is referred to as $\partial\Omega_h$ and the corresponding element boundary $\partial\mathcal{E}_E$ is divided into n_F faces F as

$$\partial\mathcal{E}_E = \bigcup_{F=1}^{n_F} \mathcal{F}_F. \tag{7}$$

Here, $\mathcal{F}_F \subset \partial\mathcal{E}_E \subset \mathbb{R}^2$ denotes a planar domain. The faces in the current configuration are defined by n_V spatial coordinates $\mathbf{x}_V$ and are assigned a unique outward normal vector $\mathbf{n}_F$. Non-degeneracy of the mesh indicates that $n_F \geq 4$ per element and $n_V \geq 3$ per face as each element E must be tetrahedral at least. The scaled boundary parameterization [7] allows us to partition the three-dimensional domain into a two-dimensional boundary domain $(\eta, \zeta) \in [-1,\ 1] \times [-1,\ 1]$ and a one-dimensional scaling direction $\xi \in [0, 1]$. Practically speaking, each polyhedron is split into its two-dimensional faces and a one-dimensional scaling direction. The

local scaling center coordinates, denoted as $\mathbf{X}_0$, are herein selected to match the coordinates of the element centroid. In order to approximate the displacement field, linear interpolation functions are employed in all three directions, resulting in a three-dimensional interpolation function for each node. The one-dimensional shape functions in scaling direction read

$$N_1(\xi) = 1 - \xi \quad \text{and} \quad N_2(\xi) = \xi, \tag{8}$$

where $N_1(\xi)$ is always regarded as the interpolation function of the scaling center, since $\xi = 0$ at the scaling center and $\xi = 1$ at the boundary. We consider three cases to cover all possible n_V per face. If a considered face is triangular ($n_V = 3$) and the section thereby tetrahedral, the shape functions of the section read

$$N_1(\xi, \eta, \zeta) = \xi(1 - \eta - \zeta), \quad N_2(\xi, \eta) = \xi\eta, \quad N_3(\xi, \zeta) = \xi\zeta, \quad N_0(\xi) = 1 - \xi. \tag{9}$$

Pyramidal sections with a quadrilateral base can be treated in the same manner, leading to

$$\begin{aligned} N_1(\xi, \eta, \zeta) &= \frac{1}{4}\xi(1 - \eta)(1 - \zeta), \quad N_2(\xi, \eta, \zeta) = \frac{1}{4}\xi(1 + \eta)(1 - \zeta), \\ N_3(\xi, \eta, \zeta) &= \frac{1}{4}\xi(1 + \eta)(1 + \zeta) \quad N_4(\xi, \eta, \zeta) = \frac{1}{4}\xi(1 - \eta)(1 + \zeta), \\ N_0(\xi) &= 1 - \xi. \end{aligned} \tag{10}$$

The third case includes every polygonal face with more than four vertices ($n_V > 4$). Here, the face with domain $\mathcal{F}_F$ is partitioned *a priori* into triangular or quadrilateral facets and the interpolation functions of Eqs. (9) and (10) can be applied, respectively. The lowest-order pressure field is approximated by a constant function and is therefore constant for the entire polyhedral element. According to [8, 10], it can be stated that volumetric locking cannot be alleviated if a non-shared pressure degree of freedom is chosen.

Using the appropriate interpolation functions for each section and considering the finite element assembly, Eqs. (4) are discretized as:

$$\underbrace{\begin{bmatrix} \mathbf{K}_{\mathrm{uu}} & \mathbf{K}_{\mathrm{up}} \\ \mathbf{K}_{\mathrm{pu}} & -\mathbf{K}_{\mathrm{pp}} \end{bmatrix}}_{\mathbf{K}_T} \begin{bmatrix} \Delta\hat{\mathbf{u}} \\ \Delta\hat{\mathbf{p}} \end{bmatrix} = \begin{bmatrix} \mathbf{f} \\ \mathbf{0} \end{bmatrix} - \begin{bmatrix} \mathbf{r}_u \\ \mathbf{r}_p \end{bmatrix}. \tag{11}$$

Note that $\mathbf{K}_{\mathrm{pp}} = \mathbf{0}$ in case of total incompressibility ($\kappa = \infty$).

4 STABILITY

In context of this work, we assume that the problem is coercive, indicating that the solvability condition (see [11])

$$\hat{\mathbf{u}}_h^{\mathsf{T}} \mathbf{K}_{\mathrm{uu}} \hat{\mathbf{u}}_h > 0 \quad \text{for all } \hat{\mathbf{u}}_h \text{ satisfying} \quad \mathbf{K}_{\mathrm{pu}} \hat{\mathbf{u}}_h = \mathbf{0} \tag{12}$$

is fulfilled. A unique displacement field $\hat{\mathbf{u}}_h$ is then guaranteed. Solvability of Eqs. (11) furthermore implies that [11]:

$$\mathbf{K}_{\mathrm{up}}\hat{\mathbf{p}}_h = \mathbf{0} \quad \text{only if} \quad \hat{\mathbf{p}}_h = \mathbf{0}, \tag{13}$$

which corresponds to the discrete inf-sup condition [12]. All nontrivial solutions to $\mathbf{K}_{\mathrm{up}}\hat{\mathbf{p}}_h = \mathbf{0}$ are spurious pressure modes and will be determined in the next section.

5 SPURIOUS PRESSURE MODES

5.1 Push-forward operation

If we recall the directional derivative

$$\mathcal{D}_p G_u \cdot \Delta p = b\left(\delta\mathbf{u},\ \Delta p\right) = \int_{\Omega_h} \delta\mathbf{E} : \frac{\partial \hat{U}}{\partial \mathbf{E}}\, \Delta p \, \mathrm{d}V, \tag{14}$$

and apply the derivative with respect to the Green-Lagrange strain tensor as

$$\frac{\partial \hat{U}}{\partial \mathbf{E}} = 2\, \frac{\partial\left(J-1\right)}{\partial \mathbf{C}} = J\mathbf{C}^{-1} = J\mathbf{F}^{-1}\mathbf{F}^{-\mathsf{T}}, \tag{15}$$

Eq. (14) can be rewritten as

$$b\left(\delta\mathbf{u},\ \Delta p\right) = \int_{\Omega_h} \delta\mathbf{E} : \mathbf{F}^{-1}\mathbf{F}^{-\mathsf{T}}\, \Delta p\, J\mathrm{d}V. \tag{16}$$

A constant interpolation function is used to interpolate the pressure and a push-forward operation is used to transfer the volume integral from the reference configuration to the current configuration. The result for an element E becomes:

$$b_E\left(\delta\mathbf{u},\ \Delta p_E\right) = \int_{\mathcal{E}_E^t} \mathrm{grad}\left(\delta\mathbf{u}\right)\mathbf{F} : \mathbf{F}^{-\mathsf{T}}\, \mathrm{d}v\, \Delta p_E \tag{17}$$

$$= \int_{\mathcal{E}_E^t} \mathrm{div}\left(\delta\mathbf{u}\right)\, \mathrm{d}v\, \Delta p_E. \tag{18}$$

Lastly, the divergence theorem is applied, leading to an integral over the element boundary:

$$b_E\left(\delta\mathbf{u},\ \Delta p_E\right) = \int_{\partial\mathcal{E}_E^t} \delta\mathbf{u}^{\mathsf{T}}\, \mathbf{n}\, \mathrm{d}a\, \Delta p_E. \tag{19}$$

Following, we focus on an arbitrary vertex ($\star$) in the interior of the mesh. This vertex is connected to d_F faces F. The approximation of one of these faces F, connected to the vertex ($\star$), is considered. The virtual displacement vector on the face F is approximated and written as:

$$\delta\mathbf{u}_h = \begin{bmatrix}\mathbf{H}_1 & \mathbf{H}_2 & \dots & \mathbf{H}_{n_V-1} & \mathbf{H}_\star\end{bmatrix} \begin{bmatrix} \delta\mathbf{u}_1 \\ \delta\mathbf{u}_2 \\ \vdots \\ \delta\mathbf{u}_{n_V-1} \\ \delta\mathbf{u}_\star \end{bmatrix}. \tag{20}$$

Here, $\mathbf{H}_V = H_V(\xi, \eta)\mathbf{I}_{3\times 3}$ includes the two-dimensional interpolation functions on the boundary. Now, the approximation of Eq. (19) can be employed and the integral can be transferred to the parameter space using the determinant of the spatial Jacobian matrix $\det\bar{\mathbf{j}}$ on the boundary:

$$b_F\left(\delta\mathbf{u}_h,\ \Delta p_E\right) = \underbrace{\sum_{V=1}^{n_V-1} \delta\mathbf{u}_V^{\mathsf{T}}\ \alpha_V\ \mathbf{n}_F\ \Delta p_E}_{b_V} + \underbrace{\delta\mathbf{u}_\star^{\mathsf{T}}\ \alpha_\star\ \mathbf{n}_F\ \Delta p_E}_{b_\star}. \tag{21}$$

We consciously split the bilinear form into $b_\star$, belonging to the local node ($\star$), and b_V, including the remaining vertices. Since both the interpolation functions and the determinant are strictly positive if we consider convex faces, the following property is fulfilled:

$$\alpha_V = \alpha_\star = \int_{-1}^{1}\int_{-1}^{1} \mathbf{H}_V^{\mathsf{T}}(\xi,\ \eta)\ \det\bar{\mathbf{j}}\ \mathrm{d}\xi\mathrm{d}\eta > 0 \quad \forall\, V. \tag{22}$$

The three stiffness entries of each degree-of-freedom of the vertex ($\star$) are solely determined by $\alpha_\star\ \mathbf{n}_F$, which means that the pressure in every element that is not attached to the local node ($\star$) is uncoupled from $\delta\mathbf{u}_\star$. This means that the investigation of the elements attached to vertex ($\star$) is sufficient in order to determine spurious pressure modes. To obtain the local stiffness matrix $\mathbf{K}_{\mathrm{up}}^\star \in \mathbb{R}^{3\times d_E}$, we can assemble the discrete bilinear operators $b_\star$ for d_E elements connected to the vertex ($\star$) as:

$$B_\star\left(\delta\mathbf{u}_\star,\ \Delta p_E\right) = \delta\mathbf{u}_\star^{\mathsf{T}} \underbrace{\begin{bmatrix}\mathbf{m}_1 & \mathbf{m}_2 & \dots & \mathbf{m}_{d_E}\end{bmatrix}}_{\mathbf{K}_{\mathrm{up}}^\star} \underbrace{\begin{bmatrix}\Delta p_1\\ \Delta p_2\\ \vdots\\ \Delta p_{d_E}\end{bmatrix}}_{\Delta\mathbf{p}^\star}. \tag{23}$$

Now that the local stiffness matrix $\mathbf{K}_{\mathrm{up}}^\star$ is determined, we can verify Eq. (13). There must exist $d_E - 3$ basis vectors in the nullspace of $\mathbf{K}_{\mathrm{up}}^\star$ since the rank-nullity theorem declares

$$\mathrm{nullity}(\mathbf{K}_{\mathrm{up}}^\star) = d_E - 3, \tag{24}$$

if we assume that $\mathrm{rank}(\mathbf{K}_{\mathrm{up}}^\star) = 3$.

5.2 Minimum of the number of intersecting elements

The easiest way to exclude basis vectors from the nullspace of $\mathbf{K}_{\mathrm{up}}^\star$ is to reduce the number of columns in the matrix. Therefore, we assume that we can construct a mesh in which any interior vertex ($\star$) is attached to $d_E = 4$ elements. From now on, it is assumed that a non-degenerate Voronoi mesh is used, which fulfills this criterion. Recalling the rank-nullity theorem, one

nontrivial nullspace vector now exists. The system of equations in Eq. (23) with $d_E = 4$ then leads to:

$$B_\star\left(\delta\mathbf{u}_\star,\ \Delta p_E\right) = \delta\mathbf{u}_\star^{\mathsf{T}} \underbrace{\begin{bmatrix}\mathbf{m}_1 & \mathbf{m}_2 & \mathbf{m}_3 & \mathbf{m}_4\end{bmatrix}}_{\mathbf{K}^\star_{\mathrm{up}}} \underbrace{\begin{bmatrix}\Delta p_1\\ \Delta p_2\\ \Delta p_3\\ \Delta p_4\end{bmatrix}}_{\Delta\mathbf{p}^\star}. \tag{25}$$

with

$$\mathbf{m}_1 = \alpha_{\star,1}\mathbf{n}_1 + \alpha_{\star,2}\mathbf{n}_2 - \alpha_{\star,6}\mathbf{n}_6, \tag{26a}$$
$$\mathbf{m}_2 = \alpha_{\star,3}\mathbf{n}_3 - \alpha_{\star,2}\mathbf{n}_2 + \alpha_{\star,4}\mathbf{n}_4, \tag{26b}$$
$$\mathbf{m}_3 = \alpha_{\star,5}\mathbf{n}_5 - \alpha_{\star,1}\mathbf{n}_1 - \alpha_{\star,4}\mathbf{n}_4, \tag{26c}$$
$$\mathbf{m}_4 = \alpha_{\star,6}\mathbf{n}_6 - \alpha_{\star,3}\mathbf{n}_3 - \alpha_{\star,5}\mathbf{n}_5. \tag{26d}$$

Here, it can be observed that 6 normal vectors occur, which belong to the $d_F = 6$ faces intersecting in the local node ($\star$) of the Voronoi mesh. In order to find the only nullspace vector $\Delta\mathbf{p}^\star_s$ of $\mathbf{K}^\star_{\mathrm{up}}$, a sequence of elementary row operations are used to bring the matrix into the reduced row echelon form (RREF):

$$\mathbf{R} = \mathrm{RREF}\left(\mathbf{K}^\star_{\mathrm{up}}\right) = \begin{bmatrix}1 & 0 & 0 & R_{14}\\ 0 & 1 & 0 & R_{24}\\ 0 & 0 & 1 & R_{34}.\end{bmatrix} \tag{27}$$

R_{14}, R_{24} and R_{34} are determined as

$$R_{14} = \frac{(\mathbf{m}_2 \times \mathbf{m}_3)\cdot\mathbf{m}_4}{(\mathbf{m}_1 \times \mathbf{m}_2)\cdot\mathbf{m}_3} \tag{28a}$$

$$R_{24} = -\frac{(\mathbf{m}_1 \times \mathbf{m}_3)\cdot\mathbf{m}_4}{(\mathbf{m}_1 \times \mathbf{m}_2)\cdot\mathbf{m}_3} \tag{28b}$$

$$R_{34} = \frac{(\mathbf{m}_1 \times \mathbf{m}_2)\cdot\mathbf{m}_4}{(\mathbf{m}_1 \times \mathbf{m}_2)\cdot\mathbf{m}_3}. \tag{28c}$$

Here, we exclude the case in which $(\mathbf{m}_1 \times \mathbf{m}_2)\cdot\mathbf{m}_3 = \mathbf{0}$. It turns out that $R_{14} = R_{24} = R_{34} = -1$. From this, we determine the only nullspace vector as the hydrostatic pressure mode:

$$\Delta\mathbf{p}^\star_s = \begin{bmatrix}\Delta\check{p} & \Delta\check{p} & \Delta\check{p} & \Delta\check{p}\end{bmatrix}^{\mathsf{T}}. \tag{29}$$

Since the aim of this work is the comparison between different element meshes regarding spurious pressure modes, the number of elements that are attached to the inner vertex ($\star$) can vary. Note that the number of nullspace vectors in $\mathbf{K}^\star_{\mathrm{up}}$ increases linearly with the number of elements intersecting in one inner local node ($\star$). On hexahedral meshes with $d_E = 8$, there exist a total of 5 nullspace basis vectors. It can be shown that these can be combined to obtain a pure checkerboard mode.

6 NUMERICAL EXAMPLE

A semicircle with quadratic cross section is considered (see Fig. 1(A)). The body is described by a Neo-Hookean nearly-incompressible material law with Young's modulus $E = 100$ and Poisson's ratio $\nu = 0.4999$. The boundary conditions are visualized in Figure 1(A). At $X_3 = 0$, homogeneous displacement boundary conditions are prescribed in the X_2- and X_3- directions. At $X_1 = 0$, the displacement is prescibed as

$$\begin{bmatrix} \bar{u}_1 \\ \bar{u}_2 \\ \bar{u}_3 \end{bmatrix} = \begin{bmatrix} 0 \\ -3.75 \\ -7.5 \end{bmatrix}. \tag{30}$$

We take advantage of the symmetry of the problem, so that it is sufficient to construct only half of the arc. In order to construct the curved mesh with different mesh patterns, the nodal coordinates $\hat{X}_1$, $\hat{X}_2$ and $\hat{X}_3$ of a reference cuboid with dimensions $B = 2$, $D = 2$, $H = \frac{9\pi}{2}$ are transformed according to

$$X_1 = \hat{X}_1 \cos\left(\frac{\hat{X}_3}{R}\right) + R \quad \text{and} \quad X_3 = \hat{X}_3 \sin\left(\frac{\hat{X}_3}{R}\right), \tag{31}$$

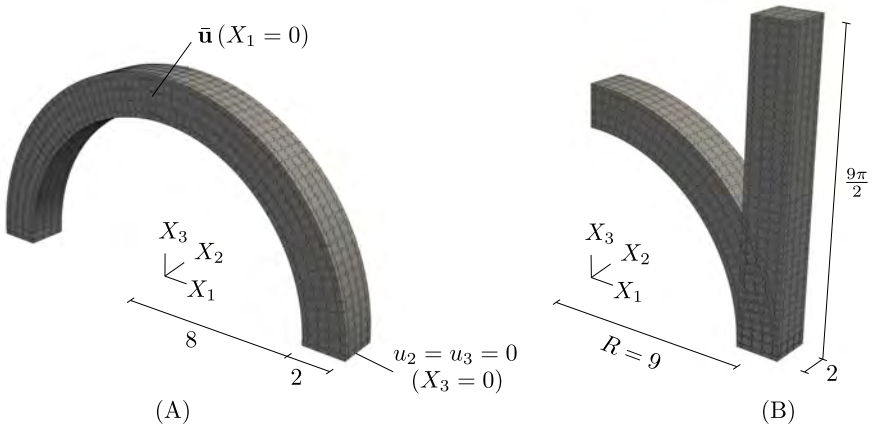

Figure 1: (A) Problem description (B) Transformation of a cuboidal mesh to the considered curved mesh.

where the reference coordinate system $\hat{X}_i$ is placed in the center of the cuboid's face at $X_3 = 0$. Note that the coordinates in the X_2-direction remain unchanged. The transformation bends the domain into a semicircle with radius $R = 9$. This allows us to construct any arbitrary mesh on the cuboid and map this mesh to the semicircle. We compare the occurrence of spurious pressure modes in our polyhedral finite element formulation on two different meshes. Both meshes are constructed using a 3D Voronoi meshing algorithm in the reference domain. The

Figure 2: Deformed configuration discretized by meshes based on $\hat{\mathcal{S}}_{\mathrm{HCB}}$ (left) and $\hat{\mathcal{S}}_{\mathrm{HEX}}$ (right).

hexahedral discretization with a total of 1024 elements can be obtained by constructing a regular grid of Voronoi sites referred to as the set $\hat{\mathcal{S}}_{\mathrm{HEX}}$, which is defined as

$$\hat{\mathcal{S}}_{\mathrm{HEX}} = \left\{-\frac{7}{8}, -\frac{5}{8}, ..., \frac{7}{8}\right\} \times \left\{-\frac{7}{8}, -\frac{5}{8}, ..., \frac{7}{8}\right\} \times \left\{\frac{9\pi}{64}, \frac{27\pi}{64}, ..., \frac{279\pi}{64}\right\}. \tag{32}$$

Here, eight elements are attached to a node in the interior of the mesh. Additionally, a bitruncated cubic honeycomb (HCB) pattern is chosen with the following seed point arrangement:

$$\hat{\mathcal{S}}_{\mathrm{HCB}} = \hat{\mathcal{S}}^1_{\mathrm{HCB}} \cup \hat{\mathcal{S}}^2_{\mathrm{HCB}} \tag{33}$$

with

$$\hat{\mathcal{S}}^1_{\mathrm{HCB}} = \left\{-\frac{3}{4}, -\frac{1}{4}, \frac{1}{4}, \frac{3}{4}\right\} \times \left\{-\frac{3}{4}, -\frac{1}{4}, \frac{1}{4}, \frac{3}{4}\right\} \times \left\{\frac{9\pi}{136}, \frac{27\pi}{136}, ..., \frac{603\pi}{136}\right\} \tag{34a}$$

$$\hat{\mathcal{S}}^2_{\mathrm{HCB}} = \left\{-1, -\frac{1}{2}, \frac{1}{2}, 1\right\} \times \left\{-1, -\frac{1}{2}, \frac{1}{2}, 1\right\} \times \left\{0, \frac{9\pi}{68}, ..., \frac{9\pi}{2}\right\}. \tag{34b}$$

The combination of these subsets ensures a maximum of four intersecting Voronoi elements for each individual node, which should suppress spurious pressure modes. The deformed configuration is depicted in Figure 2 for both mesh patterns, respectively. The discrete pressure fields are shown in Fig. 3. It can be recognized that the hexahedral mesh displays an oscillatory behavior, whereas the pressure on the honeycomb mesh is smooth and no pollution of the pressure solution is recognizable. Moreover, the pressure increment is observed in each Newton-Raphson iteration ($i = 1, 2, 3, 4, 5, 6$) of the last load step ($k = 5$). The results along the inner radius at the edge $X_2 = -1$ are shown in Figure 4. It should be noted that the angle is zero at $(X_1 = 8,\ X_3 = 0)$ and equal to $\pi/2$ at $(X_1 = 0,\ X_3 = 8)$. The stabilization effect of the honeycomb mesh is clearly visible in each Newton-Raphson iteration.

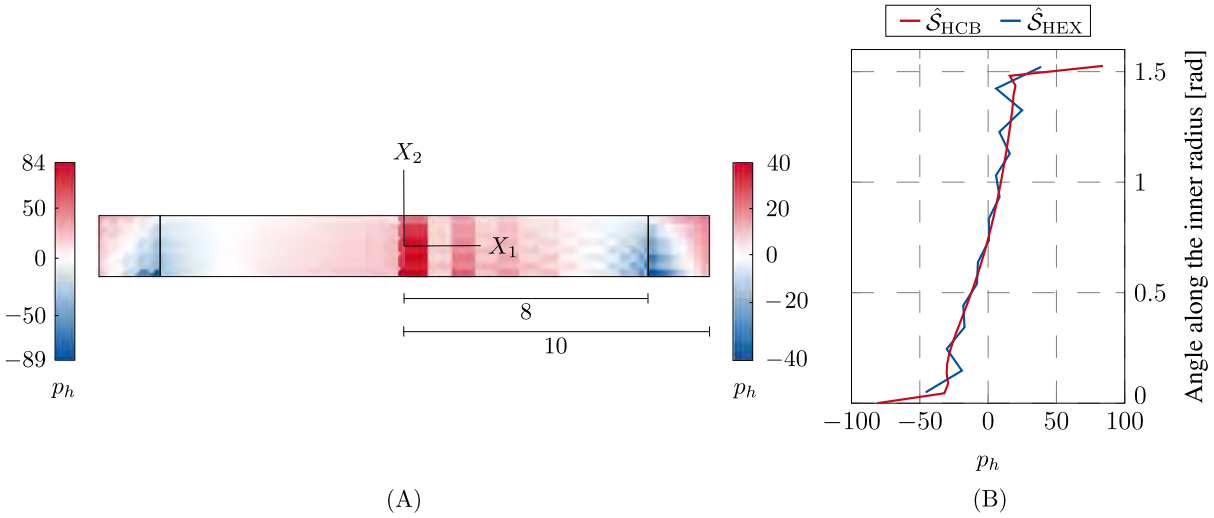

Figure 3: (A) - Bottom view onto the observed arc with prescribed displacement $\bar{\mathbf{u}}$. Honeycomb (HCB) discretization and corresponding pressure field (left), hexahedral (HEX) discretization and corresponding pressure field (right). (B) - Total pressure distribution along the inner radius at $R = 8$.

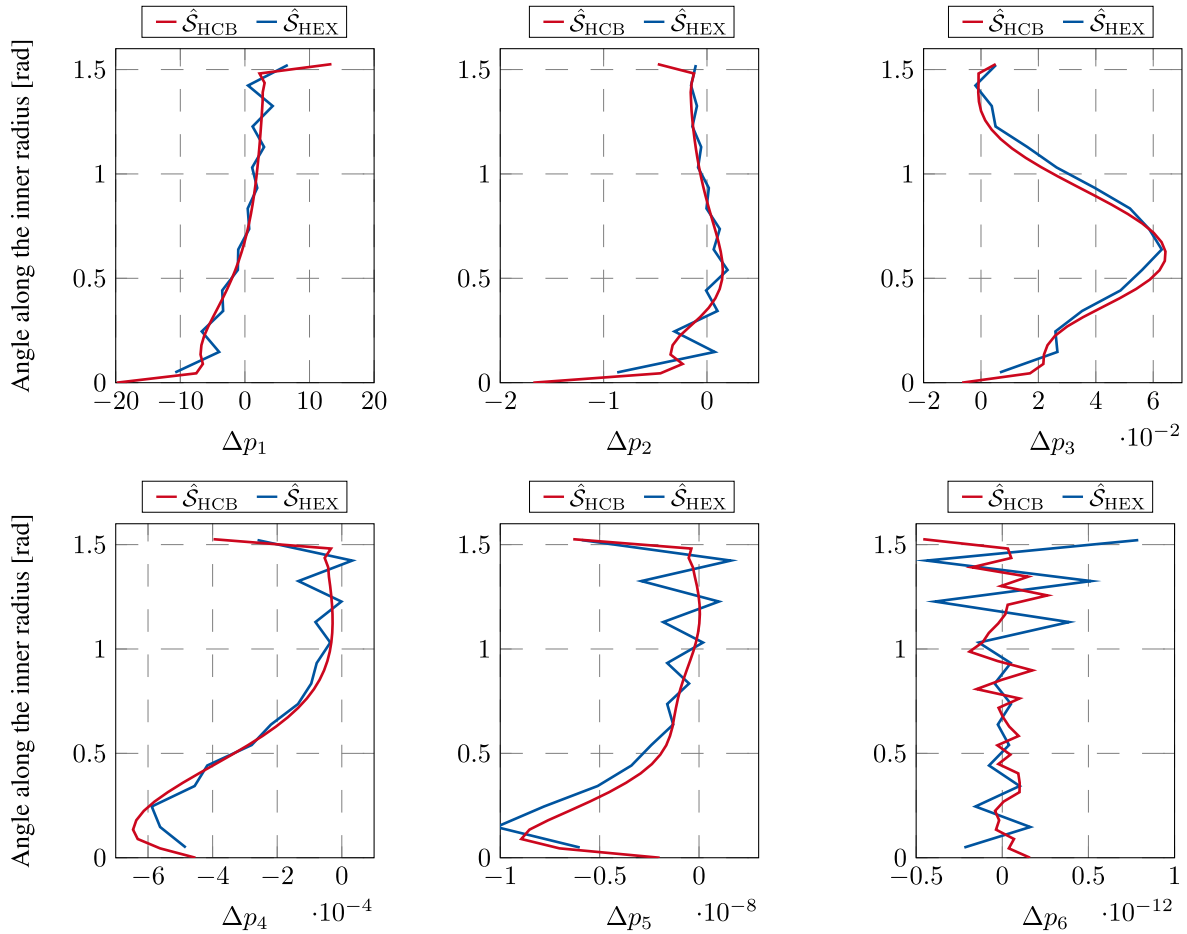

Figure 4: Pressure increment Δp_i along the inner radius during each Newton-Raphson iteration ($i = 1, 2, 3, 4, 5, 6$) of the 5^{th} load step ($k = 5$).

REFERENCES

[1] S. Reese and P. Wriggers, "A stabilization technique to avoid hourglassing in finite elasticity," *International Journal for Numerical Methods in Engineering*, vol. 48, no. 1, pp. 79–109, 2000.

[2] J.-C. Simo and F. Armero, "Geometrically non-linear enhanced strain mixed methods and the method of incompatible modes," *International Journal for Numerical Methods in Engineering*, vol. 33, no. 7, pp. 1413–1449, 1992.

[3] U. Brink and E. Stein, "On some mixed finite element methods for incompressible and nearly incompressible finite elasticity," *Computational Mechanics*, vol. 19, no. 1, pp. 105–119, 1996.

[4] O. A. Ladyzhenskaya, "The mathematical theory of viscous incompressible flow," vol. 76, 1969.

[5] I. Babuška, "The finite element method with lagrangian multipliers," *Numerische Mathematik*, vol. 20, no. 3, pp. 179–192, 1973.

[6] F. Brezzi, "On the existence, uniqueness and approximation of saddle-point problems arising from lagrangian multipliers," *Publications mathématiques et informatique de Rennes*, no. S4, pp. 1–26, 1974.

[7] C. Song, *The scaled boundary finite element method: introduction to theory and implementation*. John Wiley & Sons, 2018.

[8] B. Sauren, S. Klarmann, L. Kobbelt, and S. Klinkel, "A mixed polygonal finite element formulation for nearly-incompressible finite elasticity," *Computer Methods in Applied Mechanics and Engineering*, vol. 403, p. 115656, 2023.

[9] B. Sauren and S. Klinkel, "On the stability of mixed polygonal finite element formulations in nonlinear analysis," *International Journal for Numerical Methods in Engineering*, vol. 125, no. 9, p. e7358, 2024.

[10] B. Sauren, S. Klarmann, and S. Klinkel, *A mixed finite element formulation for arbitrary element geometries and nearly-incompressible finite elasticity*. Universitätsbibliothek der RWTH Aachen, 2022.

[11] K.-J. Bathe, *Finite element procedures*. Klaus-Jurgen Bathe, 2006.

[12] F. Auricchio, L. B. da Veiga, F. Brezzi, and C. Lovadina, "Mixed finite element methods," *Encyclopedia of Computational Mechanics Second Edition*, pp. 1–53, 2017.